

Mott insulators of ultracold fermionic alkaline earth atoms in three dimensions

Hao Song and Michael Hermele

Department of Physics, University of Colorado, Boulder, Colorado 80309, USA

We study a class of $SU(N)$ Heisenberg models, describing Mott insulators of fermionic ultra-cold alkaline earth atoms on the three-dimensional simple cubic lattice. Based on an earlier semiclassical analysis, magnetic order is unlikely, and we focus instead on a solvable large- N limit designed to address the competition among non-magnetic ground states. We find a rich phase diagram as a function of the filling parameter k , composed of a variety of ground states spontaneously breaking lattice symmetries, and in some cases also time reversal symmetry. One particularly striking example is a state spontaneously breaking lattice rotation symmetry, where the cubic lattice breaks up into bilayers, each of which forms a two-dimensional chiral spin liquid state.

I. INTRODUCTION

Ultracold atom experiment techniques enable us to vary parameters of quantum many-body systems that can hardly be changed in solid state materials.¹⁻³ For example, in solid state systems the crystal structure is selected by nature, so it is usually not easy to study the dependence of the system properties on the lattice structure. But in ultracold atom experiments the optical lattice can be chosen artificially, and its dimension and geometry can be varied. Also, we have significant freedom to select the constituent particles of a many-body system. They can be atoms or molecules, bosons or fermions, and so on. Different atoms or molecules interact with one another quite differently, and in some cases the interactions can be tuned with electric or magnetic field. So cold atoms promise to allow us explore systems in new parameter regimes, or even systems that have no analog in solid state materials.

Fermionic⁴ ultracold alkaline earth atoms (AEAs) have attracted significant interest recently due to their unique properties,⁵⁻²⁵ and experimental progress developing the study of many-body physics in AEA systems has been rapid²⁶⁻⁴¹. One key feature of AEAs is the presence, to an excellent approximation, of $SU(N)$ spin rotation symmetry, where $N = 2I + 1$ and I is the nuclear spin.^{5,6} This occurs in both the 1S_0 ground state and a metastable 3P_0 excited state, where the electronic angular momentum $J_e = 0$ and the hyperfine interaction is thus quenched. This leads to the nuclear-spin-independence of the s-wave scattering lengths between AEAs, and to $SU(N)$ spin rotation symmetry. When loaded in optical lattices, AEA systems are described by $SU(N)$ -symmetric Hubbard models.⁵ Since the largest I obtained using AEA is $I = 9/2$ in the case of ^{87}Sr , $N \leq 10$ is the experimentally accessible regime. Different setups are possible, and as a result, $SU(N)$ versions of several models, such as the Kugel-Khomskii model, the Kondo lattice model, and the Heisenberg spin model, can be realized with AEAs as special or limiting situations of the more general Hubbard model.

Among these models, we focus in this paper on $SU(N)$ antiferromagnetic Heisenberg models, which describe the Mott insulator phase of fermionic AEAs in optical lat-

tices. More specifically, we are concerned with such models on three dimensional lattices, which have received much less attention than the one- and two-dimensional cases. Because of the enlarged symmetry, the number of spins needed to make a singlet, denoted by k , is in general larger than two. In the simplest AEA Heisenberg model with one atom per lattice site, $k = N$. In addition, in the semiclassical limit of the Heisenberg models that can be realized using AEAs, two neighboring classical spins prefer energetically to be *orthogonal* rather than anti-parallel.⁷ Both these features contrast with $SU(2)$ antiferromagnetic Heisenberg models appropriate for some solid state materials, where neighboring *pairs* of spins can and tend to form singlet valence bonds, and neighboring classical spins prefer to be anti-parallel. We can thus expect new physics in $SU(N)$ Heisenberg models with $k > 2$.

Indeed, Ref. 7 argued that the underconstrained nature of the semiclassical limit makes magnetic order unlikely for large enough N on any lattice, and non-magnetic ground states are more likely. While the models of physical interest are challenging to study directly, information about possible non-magnetic ground states can be obtained in a large- N limit designed to address the competition among such states.⁴²⁻⁴⁴ Such a large- N study was carried out for AEA $SU(N)$ Heisenberg models on the two-dimensional square lattice in Refs. 7 and 13. One possible non-magnetic state is a cluster state, where clusters of k (or a multiple of k) neighboring spins form singlets; this is a generalization of a valence bond state. Another possibility is a spin liquid state, where full translational symmetry is preserved. For the simplest AEA Mott insulators (with 1S_0 ground state atoms only), on the square lattice the large- N study finds cluster states for $k \leq 4$, and a chiral spin liquid (CSL) state for $k \geq 5$.^{7,13} The CSL spontaneously breaks time-reversal (\mathcal{T}) and parity (\mathcal{P}) symmetries, and can be viewed as a magnetic analog of the fractional quantum Hall effect (FQHE), with similar exciting properties of quasiparticles with anyonic statistics, gapless chiral edge states, and so on.⁴⁵⁻⁴⁷ CSLs have also been found in a variety of other exactly solvable models.⁴⁸⁻⁵⁴

The CSL is, however, intrinsically a two-dimensional phenomenon, so it is natural to ask about non-magnetic

ground states of $SU(N)$ antiferromagnetic Heisenberg models in three dimensions. In this paper, we address this question by a large- N study of a class of $SU(N)$ Heisenberg models on the simple cubic lattice, and find a rich phase diagram as a function of k including cluster states, but also more intricate inhomogeneous states. Most strikingly, for $k = 7, 10$ we find a bilayer CSL state, where the lattice spontaneously breaks into weakly coupled square bilayers (thus breaking rotational symmetry), each of which is a two-dimensional CSL. We thus find that the CSL survives to three dimensions, relying on spontaneous symmetry breaking that results in effective quasi-two-dimensionality.

We now define our model before briefly surveying some related prior work. We consider a fermionic AEA with N spin species, and put m 1S_0 ground state atoms on each site of a simple cubic lattice (see Sec. II for more details). The atoms form a Mott insulator due to repulsive on-site interactions. For simplicity, we consider the case of dominant on-site interaction, so that the spin degrees are governed by a antiferromagnetic superexchange interaction restricted to nearest neighbors. While $m = 1$ is the most interesting situation since it best avoids three-body losses, we also consider more generally the case where $\frac{N}{m}$ is an integer. Then, the minimum number of spins needed to make a $SU(N)$ singlet is $k = \frac{N}{m}$. We sometimes refer to k as the filling parameter. When $m = 1$, each spin transforms in the fundamental representation of $SU(N)$. In the large- N limit, N is taken large while k is held fixed. Given the physical interpretation of k , we thus view the large- N results for a given k as a guide to the physics of the physically realizable model with $m = 1$ and $N = k$.

Our focus is on three spatial dimensions, but we note that one-dimensional $SU(N)$ Heisenberg spin chains have been solved exactly for the case $m = 1$,⁵⁵ and the effective field theory of such chains is understood for general m .⁵⁶ The latter analysis shows that gapless states with quasi-long-range order, as well as gapless cluster states, occur in one dimension. In two dimensions, early studies of $SU(N)$ antiferromagnets focused on models where two neighboring spins can be combined to form a singlet. This work included the models we consider for the case $m = N/2$,^{42,43} but also other $SU(N)$ antiferromagnets with spins transforming in two distinct conjugate representations on the two sublattices of a bipartite lattice.⁴⁴ Models with $k = 2$ have also received attention more recently,^{10,23,57,58} and two dimensional models with $k > 2$ have been studied^{7,11–13,15,24,25,59–64} (see Ref. 13 for a more detailed discussion of some of these prior works). The $m = 1$, $N = 3$ model on the square lattice is magnetically ordered,¹¹ and there is also evidence for magnetic order for $m = 1$, $N = 4$.¹² Only a little attention has been devoted to the case of three dimensions,^{11,59,65} but we note the high temperature series study of Ref. 65, where the $m = 1$ model on the simple cubic lattice was studied for various values of N , and it was found that increasing N led to a decreased tendency toward magnetic

order. References 66 and 67 studied effective models for four-site singlet clusters on the cubic lattice. Finally, we note that high-spin quantum magnets can also be realized using ultra-cold alkali atoms. While N -component such systems do not generically obey $SU(N)$ spin symmetry, the symmetry is enhanced above $SU(2)$,⁶⁸ and such systems have received significant attention.^{68–74}

In Sec. II, we review the large- N solution to our model. This is followed by presentation of the large- N results for $k = 2, \dots, 10$ in Sec. III, together with a discussion of how those results are obtained and checked. As part of that discussion, we develop an interesting relation between some cubic lattice saddle points (including the ground state saddle points for $k = 5, \dots, 10$) and saddle points on the single-layer square lattice with filling parameter $k' = k/2$. The paper concludes with a discussion of the striking properties of the bilayer CSL state (Sec. IV).

II. THEORETICAL MODEL

The $SU(N)$ Hubbard model

$$\mathcal{H}_{Hubbard} = -t \sum_{\langle rr' \rangle} (c_r^{\alpha\dagger} c_{r'\alpha} + h.c.) + (U/2) \sum_r (c_r^{\alpha\dagger} c_{r\alpha} - m)^2, \quad (1)$$

describes the behavior of fermionic AEAs on an optical lattice.⁵ Here $c_r^{\alpha\dagger}$ and $c_{r\alpha}$ are the creation and annihilation operators for the fermionic atom with spin state α at site r . The sum in the first term is over nearest-neighbor pairs of lattice sites. We will primarily consider the simple cubic lattice. We choose the number of atoms so that m is the integer number of atoms per lattice site. There are N spin states, $\alpha, \beta = 1, 2, \dots, N$, and spin indices are summed over when repeated. The total number of lattice sites is N_s . The operator $c_r^{\alpha\dagger}$ transforms in the fundamental representation of $SU(N)$, while $c_{r\alpha}$ transforms in the anti-fundamental representation, which is related to the fundamental by complex conjugation. The upper and lower positions of the Greek indices are used to indicate the distinction between these two representations (they are unitarily equivalent only for $N = 2$).

As is well known, the $SU(2)$ Heisenberg model can be obtained as a low energy effective description of the $SU(2)$ Hubbard model when $U \gg t$. The generalization to the $SU(N)$ version is straightforward. In second order degenerate perturbation theory, one obtains the $SU(N)$ antiferromagnetic Heisenberg model defined by the Hamiltonian

$$\mathcal{H} = -J \sum_{\langle rr' \rangle} (f_r^{\alpha\dagger} f_{r'\alpha}) (f_{r'\beta}^{\beta\dagger} f_{r\beta}), \quad (2)$$

with the Hilbert space restricted by $f_r^{\alpha\dagger} f_{r\alpha} = m$, and $J = 2t^2/U > 0$. We now use $f_r^{\alpha\dagger}$ rather than $c_r^{\alpha\dagger}$ to denote the fermion creation operator, to emphasize that once we

pass to the Heisenberg model, the fermions do not move from site to site. This is important, because the structure of the large- N mean-field theory is that of a hopping Hamiltonian for the $f_r^{\alpha\dagger}$ fermions, but it is not correct to interpret this hopping as motion of atoms. Instead, in the large- N mean-field theory, the $f_r^{\alpha\dagger}$ fermions are spinons, fractional particles that may be either confined or deconfined depending on the nature of fluctuations about a mean-field saddle point. See Ref. 13 for further discussion of this point.

On each site, there are m atoms that form a $SU(N)$ spin. The Hamiltonian (2) defines an antiferromagnetic interaction, since by rearranging the fermion operators it can be written as

$$\mathcal{H} = J \sum_{\langle rr' \rangle} \hat{S}_\alpha^\beta(r) \hat{S}_\beta^\alpha(r'), \quad (3)$$

where $\hat{S}_\alpha^\beta(r) = f_r^{\beta\dagger} f_{r\alpha}$ flips the spin on site r .

We study this model on the simple cubic lattice, the simplest three dimensional case, with varying parameters N and m . While we consider more general parameter values, $m = 1$ is the case of greatest physical interest because putting only one atom on each site best avoids potential issues due to three body loss. The largest N that can be obtained using alkaline earth atoms is $N = 10$ in the case of ^{87}Sr .

Based on a semiclassical analysis, Ref. 7 argued that for large enough N , magnetic ordering is unlikely on any lattice. The argument proceeds in the semiclassical limit, where a lower bound on the dimension of the ground state manifold is derived. For $N > N_c$, where N_c depends on the lattice coordination number, the ground state manifold is extensive, meaning its dimension is proportional to the number of lattice sites. This situation occurs in some geometrically frustrated systems and is likely to lead to a strong or complete suppression of magnetic order⁷⁵, even in the semiclassical limit that favors magnetic order by construction. Therefore, non-magnetic ground states are likely when $N > N_c$. For the square lattice $N_c = 3$,⁷ and the argument is easily extended to find $N_c = 4$ on the cubic lattice.

Ideally, we would like to predict the properties of the $SU(N)$ antiferromagnetic Heisenberg model on cubic lattice for $N \leq 10$, $m = 1$. But this is extremely challenging. Instead, following the work of Refs. 7 and 13, we apply a large- N limit in which the model becomes exactly solvable, and which allows us to address the competition among different non-magnetic ground states. We fix the ratio $k = \frac{N}{m}$ (for integer k), while taking both $N \rightarrow \infty$ and $m \rightarrow \infty$. We shall sometimes refer to k as the filling parameter. For each k we thus obtain a sequence of models ($N = k, m = 1$); ($N = 2k, m = 2$), and so on. For every model in this sequence, k is the minimum number of spins needed to form a singlet, and it is thus reasonable that the large- N limit may capture the physics of the case $N = k, m = 1$ of greatest interest.

To proceed with the large- N solution, one goes to a functional integral representation, where the partition

function is

$$Z = \int \mathcal{D}\chi \mathcal{D}\chi^* \mathcal{D}\lambda \mathcal{D}\bar{f} \mathcal{D}f e^{-S}, \quad (4)$$

where

$$\begin{aligned} S = & \int_\tau \sum_r \bar{f}_r^\alpha \partial_\tau f_{r\alpha} + N \int_\tau \sum_{\langle rr' \rangle} \frac{|\chi_{rr'}|^2}{\mathcal{J}} \\ & + \int_\tau \sum_{\langle r, r' \rangle} (\chi_{rr'} \bar{f}_r^\alpha f_{r'\alpha} + h.c.) \\ & + i \int_\tau \sum_r \lambda_r (\bar{f}_r^\alpha f_{r\alpha} - m). \end{aligned} \quad (5)$$

The field $\chi_{rr'}$ is a complex Hubbard-Stratonovich field that has been used to decouple the exchange interaction, and λ_r is a real Lagrange-multiplier field enforcing the $f_r^{\alpha\dagger} f_{r\alpha} = m$ constraint. The fermion fields f and \bar{f} are the usual Grassmann variables. We have introduced $\mathcal{J} = NJ$; \mathcal{J} is held fixed in the large- N limit. Finally, $\int_\tau \equiv \int_0^\beta d\tau$. We shall always be interested in zero temperature, *i.e.* $\beta \rightarrow \infty$.

When both N and m are large, the effective action for χ and λ (obtained upon integrating out fermions), is proportional to N (since $m \sim N$), and therefore the saddle point approximation becomes exact for the χ and λ integrals. We can therefore replace χ and λ by their saddle-point values, $\chi_{rr'} \rightarrow \bar{\chi}_{rr'}$ and $\lambda_r \rightarrow i\mu_r$. The saddle-point equations are

$$m = \langle f_r^{\alpha\dagger} f_{r\alpha} \rangle, \quad (6)$$

$$\bar{\chi}_{rr'} = -\frac{\mathcal{J}}{N} \langle f_r^{\alpha\dagger} f_{r'\alpha} \rangle. \quad (7)$$

The above averages are taken in the ground state of the saddle-point (or mean-field) Hamiltonian

$$\begin{aligned} \mathcal{H}_{MFT} = & N \sum_{\langle rr' \rangle} \frac{|\bar{\chi}_{rr'}|^2}{\mathcal{J}} + m \sum_r \mu_r \\ & + \sum_{\langle rr' \rangle} (\bar{\chi}_{rr'} f_r^{\alpha\dagger} f_{r'\alpha} + h.c.) - \sum_r \mu_r \hat{n}_r, \end{aligned} \quad (8)$$

where $\hat{n}_r \equiv f_r^{\alpha\dagger} f_{r\alpha}$.

The ground state is determined by finding the global minimum of $E_{MFT}(\{\chi_{rr'}\}, \{\mu_r\})$, the ground state energy of \mathcal{H}_{MFT} , as a function of the χ 's and μ 's, with the constraint that the saddle point equations must be satisfied. While any solution of the saddle point equations gives an extremum of the energy, in general it is not trivial to find the global minimum. To address this question, we follow Refs. 7 and 13 and apply the combination of analytical and numerical techniques developed there, as described below in Sec. III.

III. LARGE- N GROUND STATES

A. Summary of the large- N mean-field results

In the limit $N \rightarrow \infty$, the ground states are characterized entirely by the mean-field saddle point values of $\chi_{rr'}$ and μ_r . The most important information is contained in $\chi_{rr'}$, since typically it is possible for a given $\chi_{rr'}$ to find μ_r so that the density constraint Eq. (6) is satisfied. For instance, depending on whether two sites are connected (i.e. whether there is a set of nonzero $\chi_{rr'}$'s forming a path connecting the two sites), we can tell whether the spins on the two sites are correlated or not. Not all the information contained in $\chi_{rr'}$ is physical. The theory has a $U(1)$ gauge redundancy

$$\begin{aligned} f_{r\alpha} &\rightarrow f_{r\alpha} e^{i\phi(r)} \\ \chi_{rr'} &\rightarrow \chi_{rr'} e^{i(\phi(r) - \phi(r'))}, \end{aligned} \quad (9)$$

so the physical information is contained in the following gauge-invariant quantities: (1) magnitude $|\chi_{rr'}|$ and (2) flux $\Phi = a_{12} + a_{23} + a_{34} + a_{41}$ through each plaquette, where 1, 2, 3, 4 indicates the four vertices of a plaquette and $a_{rr'}$ is the phase of the $\chi_{rr'}$, i.e. $\chi_{r'r} = e^{ia_{rr'}} |\chi_{rr'}|$. (Since $\chi_{r'r} = \chi_{rr'}^*$, $a_{r'r} = -a_{rr'}$.)

Based on a combination of analytical and numerical techniques described below, we found the ground state configuration of $\chi_{rr'}$ and μ_r for $k = 2, \dots, 10$. These results, which are rigorous for $k = 2, 3, 4$, are summarized in Table I. Different types of ground states are found depending on k . In an n -site cluster pattern of $\chi_{rr'}$, the lattice is partitioned into n -site clusters such that $\chi_{rr'} \neq 0$ only if r, r' lie in the same cluster. We call the corresponding ground state a n -site cluster state, which can be viewed as a generalization of a valence bond state (2-site cluster state, in our terminology). Similarly, a bilayer pattern partitions the lattice into bilayers, and $\chi_{rr'}$ is only nonzero for r, r' in the same bilayer. The corresponding ground states are called bilayer states. In all cases, each bilayer is comprised of two adjacent $\{100\}$ lattice planes. A CSL bilayer is a special kind of bilayer state, where in each bilayer

$$|\chi_{rr'}| = \begin{cases} \chi, & \langle rr' \rangle \text{ lies within either layer;} \\ \frac{\chi}{k}, & \langle rr' \rangle \text{ connects the two layers.} \end{cases} \quad (10)$$

Moreover, there is a uniform flux

$$\Phi = \frac{4\pi}{k} \quad (11)$$

through each plaquette lying within the two layers, and zero flux through each plaquette perpendicular to the two layers. This situation corresponds to a uniform orbital magnetic field applied perpendicular to the layers. At the mean-field level, a single CSL bilayer exhibits integer quantum Hall effect with $\nu = 1$ for each spin species of $f_{r\alpha}$ fermion.

k	Large- N ground state	Sketch of $\chi_{rr'}$	Energy
2	2/4-site cluster	Fig. 1a	-0.125
3	6-site cluster	Fig. 1b	-0.0833333
4	4/8-site cluster	Fig. 1c	-0.0625
5	20-site cluster	Fig. 2a, 2b	-0.0445021
6	12-site cluster	Fig. 2c, 2d	-0.0347222
7	CSL bilayer	Fig. 2e, 2f	-0.0273888
8	8-site cluster	Fig. 2g, 2h	-0.0234375
9	Inhomogeneous bilayer	Fig. 2i, 2j	-0.0188265
10	CSL bilayer	Fig. 2e, 2f	-0.01577

TABLE I. Ground state saddle-point patterns of $\chi_{rr'}$, and the corresponding energies in units of $N\mathcal{J}N_s$ for $k = 2, 3, \dots, 10$. The different types of large- N ground states are described in the text, and depicted in figures as indicated.

To fully understand the different ground states, one has to go beyond the $N = \infty$ or mean-field description. At the mean-field level, the number of ground state arrangements of clusters or bilayers on the cubic lattice diverges with the system size. For example, there are usually many ways to tile the lattice with a given type of n -site cluster. Also, in the CSL bilayer state, the direction of flux can be chosen independently in each bilayer without affecting the $N = \infty$ ground state energy. Such degeneracies can be resolved by computing the first correction (perturbative in $1/N$) to the ground state energy;⁴⁴ these calculations are left for future work.

In cluster states, another important effect of fluctuations is to confine the $f_{r\alpha}$ fermions; the cluster states are thus ‘‘ordinary’’ broken symmetry states, without exotic excitations. A more extensive discussion of fluctuations appears in Ref. 13, and the resulting physical properties of the CSL bilayer are discussed in Sec. IV. We have not considered the effect of fluctuations in the $k = 9$ inhomogeneous bilayer ground state.

B. Detailed descriptions of the mean-field ground states

We now discuss the mean-field ground states for each value of k . We note that, for $k \geq 5$, we cannot rule out the possibility that the true ground state is lower in energy than the ground state we found. The ground-state clusters for $k = 2, 3, 4$ are depicted in Fig. 1. These are essentially the same as found in the two-dimensional square lattice,^{7,13} but going to the three-dimensional cubic lattice permits a greater variety of clusters for $k = 3, 4$.

It was noted in Ref. 44 that for $k = 2$ there is actually a *continuous* family of $N = \infty$ ground states, which can be seen for a single square plaquette as shown in Fig. 1a and discussed in the figure caption. This continuous ground state degeneracy is also resolved by the order- $1/N$ corrections to the ground state energy.⁴⁴ We found that a similar continuous degeneracy occurs for $k = 4$ on a single cube (see Fig. 1c). As in the figure, consider a single cube with flux Φ_t through the top and bottom plaquettes

(*i.e.*, those lying in the xy -plane), and flux Φ_s through the side plaquettes (*i.e.*, those lying in the xz - and yz -planes). Flux passing from the center of the cube to the outside is taken positive. In order to reach the ground state we must have $2\Phi_t + 4\Phi_s = \pm 2\pi$; we choose the positive sign without loss of generality. We let $\Phi_t = 4u$ and $\Phi_s = \pi/2 - 2u$; a ground state is obtained if we restrict $0 \leq u \leq \pi/2$. In this situation the magnitude $|\chi_{rr'}$ will generally differ on vertical bonds and other bonds [shaded light (pink) and dark (blue), respectively, in Fig. 1]. The energy is minimized and saturates the lower bound when

$$\frac{|\chi_{\text{light}}|}{|\chi_{\text{dark}}|} = 2\sqrt{\cos u \sin u}. \quad (12)$$

The ground-state patterns of $\chi_{rr'}$ for $5 \leq k \leq 10$ are shown in Fig. 2. For $k = 5, 6, 8$ we again find cluster ground states. The case $k = 8$ is particularly simple; there, each cluster is a fully symmetric cube with $|\chi_{rr'}|$ constant on every bond, and no flux through the cube faces. The $k = 5$ and $k = 6$ clusters are conveniently thought of as obtained by stacking two single-layer clusters vertically, and connecting them via the vertical bonds. For $k = 5$ each cluster is a stack of two ten-site T-shaped objects. The $k = 6$ clusters are obtained by stacking two $k = 3$ ground state clusters (see Fig. 1b). In the $k = 5, 6$ cases, our numerical calculations find evidence for a continuous family of degenerate ground states within each cluster, as for the 4-site $k = 2$ clusters and 8-site $k = 4$ clusters (Fig. 1). Unlike in those cases, however, we have not been able to find a simple parametrization of the degenerate ground states.

For $k = 7, 9, 10$, we find bilayer ground states, with the CSL bilayer saddle point described above occurring for $k = 7, 10$. The $k = 9$ ground state is more complicated, spontaneously breaking translation symmetry within each bilayer. Time reversal symmetry is broken as well by a complicated pattern of fluxes. It is interesting to note that *all* the $5 \leq k \leq 10$ ground states have a bilayer structure, as the clusters for $k = 5, 6, 8$ can be arranged into bilayers (see right column of Fig. 2). In addition, the two square lattice layers of each bilayer have identical $\chi_{rr'}$, there is zero flux on the “vertical” plaquettes connecting the two layers, and the vertical bonds have magnitude $|\chi_{rr'}| = \mathcal{J}/k$.⁷⁶ As discussed below, this simple structure allows us to exploit a useful relation with the single-layer square lattice at filling parameter $k' = k/2$.

C. Obtaining the mean-field results

We now describe how the large- N ground states were determined. As on the square lattice,^{7,13} the results for $k = 2, 3, 4$ are rigorous, and are obtained by applying a lower bound on E_{MFT} obtained by Rokhsar for $k = 2$,⁷⁷ and generalized to $k > 2$ (with a stronger bound holding for bipartite lattices) in Refs. 7 and 13. Cluster states for $k = 2, 3, 4$ on the square^{7,13} and cubic lattices saturate

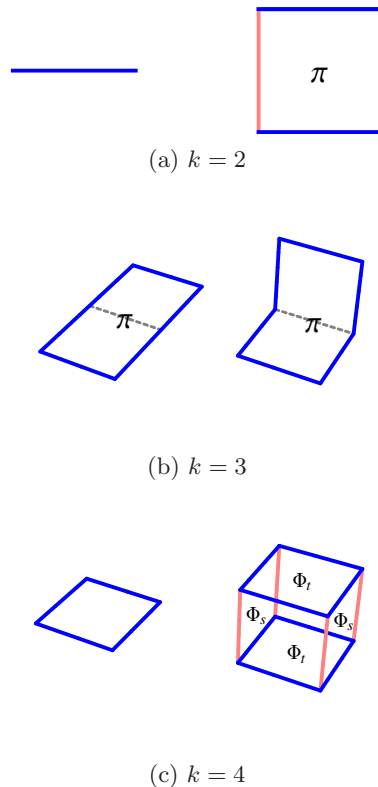


FIG. 1. Ground-state clusters for $k = 2, 3, 4$. Shaded bonds are those with $\chi_{rr'} \neq 0$. Bonds with different shading (or color in online version) may have different magnitudes $|\chi_{rr'}|$. (a) The $k = 2$ ground state clusters are dimers and square plaquettes. The square plaquette is pierced by π -flux, and the ratio of $|\chi_{rr'}|$ on light (pink online) and dark (blue online) bonds can be chosen arbitrarily. Setting $|\chi_{rr'}| = 0$ on the two light (pink) bonds breaks the plaquette into two dimers. (b) The $k = 3$ ground state cluster is a 6-site chain pierced by π -flux. On the cubic lattice, such chains can exist either as a flat rectangular loop (left), or as the same loop bent by 90° in the middle (right). In both cases, $\chi_{rr'} = 0$ on the dashed bond passing through the middle of the loop. (c) The $k = 4$ ground state clusters are square plaquettes and 8-site cubes with Φ_s -flux through the side plaquettes and Φ_t -flux through top and bottom plaquettes. There is a continuous one-parameter family of ground states on an 8-site cube, described in the text.

this lower bound. A necessary condition for saturation on a bipartite lattice is that the mean-field single-particle energy spectrum must be completely flat, with only three energies $0, \pm\epsilon$ occurring in the spectrum, and with energy $-\epsilon$ states filled and others empty.^{7,13} We believe that this kind of spectrum can only be produced by a cluster state. Moreover, for larger clusters (and thus with increasing k), it becomes harder to arrange for a spectrum containing only three energies. While we do not have a rigorous proof, we believe saturation is impossible for $k > 4$ on the square and cubic lattices.

For $k \geq 5$, we resort to a numerical approach to find the ground states. We employ the self-consistent min-

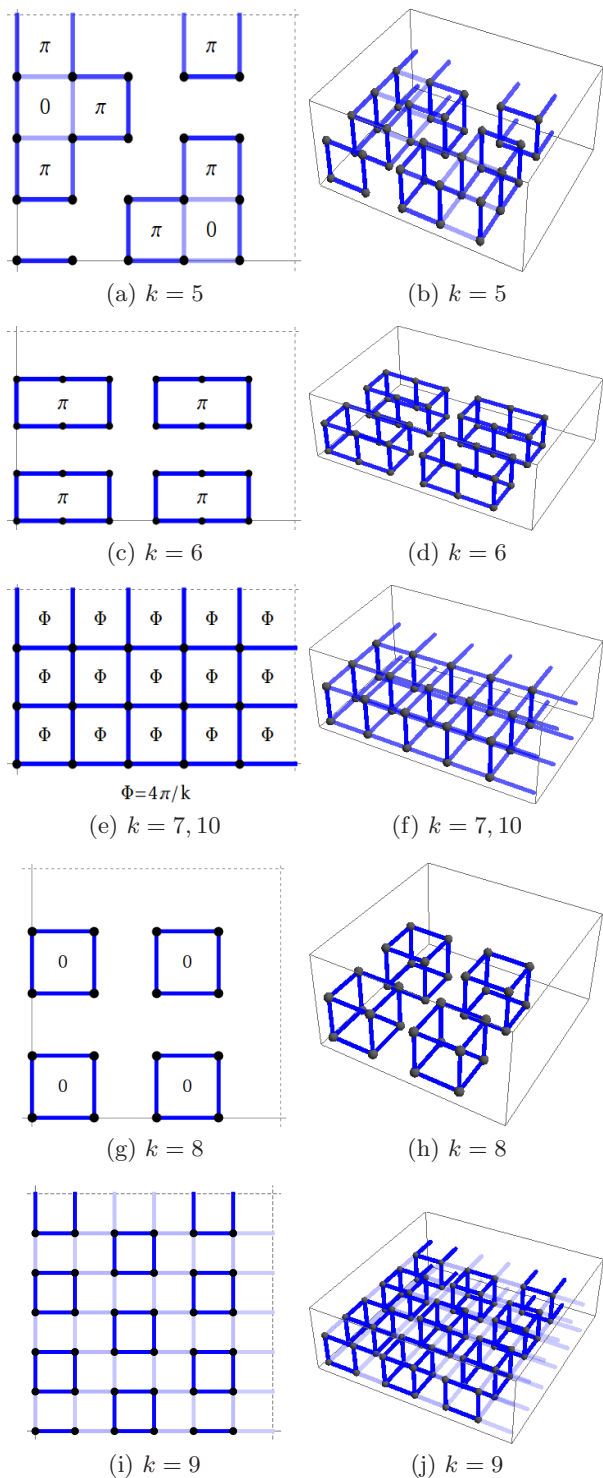


FIG. 2. Ground-state saddle point configurations of $\chi_{rr'}$ for $k = 5, 6, \dots, 10$. The right column is a three-dimensional view of each configuration, with larger magnitude $|\chi_{rr'}$ indicated by darker shading. All these saddle points can be viewed as bilayer structures, with $\chi_{rr'}$ identical on top and bottom layers. The left column thus shows $|\chi_{rr'}$ on a single layer, with fluxes indicated except for $k = 9$, where the fluxes are generally non-zero but follow a complicated pattern. Also, for $k = 5, 6$ the fluxes and $|\chi_{rr'}$ can be changed continuously within a single cluster without affecting the energy; only the simplest configurations are shown.

imization (SCM) algorithm developed in Refs. 7 and 13, which proceeds as follows (see Ref. 13 for more details):

- 1: Start with $\mu_r = 0$ and a randomly generated configuration of $\chi_{rr'}$.
- 2: Adjust μ_r to satisfy the saddle-point equation

$$\langle f_r^{\alpha\dagger} f_{r\alpha} \rangle = m, \quad \text{for all } r. \quad (13)$$

μ_r is determined by a multidimensional Newton's method.^{7,13,78} Stop if no solution is found.

- 3: Generate a new $\chi_{rr'}$ using the saddle-point equation

$$\chi_{rr'} = -\frac{\mathcal{J}}{N} \langle f_r^{\alpha\dagger} f_{r\alpha} \rangle. \quad (14)$$

- 4: Go back to step 2 until $\chi_{rr'}$ and μ_r converge.

As long as step 2 is successful, the energy E_{MFT} is guaranteed to decrease with each iteration of the SCM algorithm.^{7,13} But a random initial configuration of $\chi_{rr'}$ does not necessarily converge to the ground state, and can instead converge to a local minimum of E_{MFT} . Therefore, in order to find the ground state, we need to try as many independent random initial configurations of $\chi_{rr'}$ as possible. For those random initial configurations resulting in the lowest energies, we found extremely good convergence in E_{MFT} by the time the SCM procedure is stopped (typically after 300 iterations), and effects of randomness on the reported values of E_{MFT} are thus entirely negligible.

To improve the performance of the SCM algorithm, we define $\chi_{rr'}$ with μ_r within some fixed unit cell, which is then repeated periodically to cover a finite-size $L_x \times L_y \times L_z$ lattice with periodic boundary conditions. For simplicity, we always choose the unit cell to be a rectangular prism with edge lengths $l_{x,y,z}$ (see Fig. 3), with primitive Bravais lattice vectors parallel to the edges of the rectangular prism.⁷⁹ For each value of k , we choose the minimum linear system size $L = \min(L_x, L_y, L_z)$ to be as large as possible given the constraints of our available computing resources and the need to try a reasonably large number of different random initial conditions. In some cases we also considered larger system sizes, especially when we found competing saddle points very close in energy. A more careful study of finite-size effects would be desirable, but due to the above constraints we leave this for future work. Table II displays the range of unit cell dimensions studied for each value of k , as well as the number of random initial conditions tried for each cell, and the minimum linear system size L .

D. Relation between bilayer states and square lattice saddle points

As noted above, the ground states for $5 \leq k \leq 10$ can all be viewed as bilayer states, which means that such saddle points can also be obtained by a studying

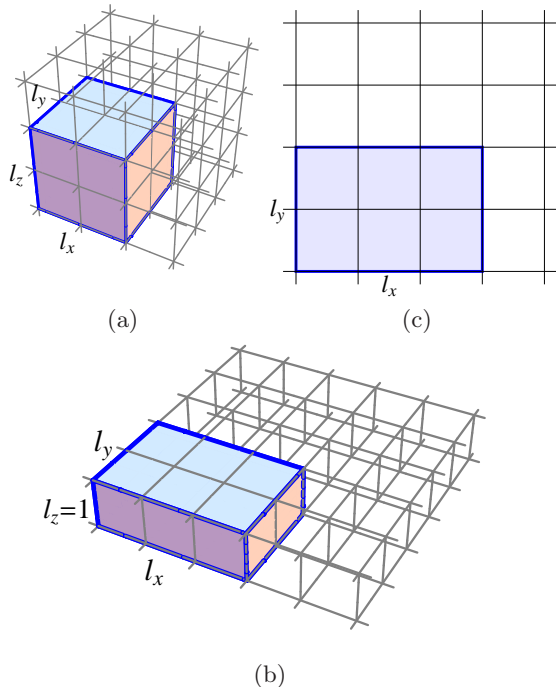


FIG. 3. Unit cells used for SCM calculations on the cubic lattice (a), single bilayer (b), and single-layer square lattice (c). In the cubic case the primitive Bravais lattice vectors are chosen parallel to the edges of the rectangular prismatic unit cell. The analogous statement is true for the bilayer and single-layer cases, with primitive Bravais lattice vectors parallel to the $l_{x,y}$ edges of the unit cell.

the large- N Heisenberg model on a single bilayer. We have also carried out SCM numerical calculations in this geometry (see Table II and Fig. 3 for more information); this is computationally cheaper than the cubic lattice SCM calculations, and provides a useful check on those results. These bilayer SCM calculations find the same ground states as the corresponding cubic lattice calculations, except for $k = 9$, where the bilayer calculation finds a lower-energy state that can then be extended to a cubic lattice saddle point. Presumably, this saddle point would also be found by SCM on the cubic lattice with enough runs using independent random initial conditions.

There is an interesting relation between certain saddle points of a single bilayer, and corresponding saddle points of a single-layer square lattice, but with filling parameter $k' = k/2$. The cubic lattice ground states for $5 \leq k \leq 10$ are all of this type. We label the sites of a single bilayer by (r, i) , where $i = 1, 2$ is the layer index, and r labels the square lattice sites within each layer. There are $N_s = 2N_s^{2d}$ lattice sites, where N_s^{2d} is the number of sites in a single layer. Consider a saddle point where

$$\chi_{r1,r'1} = \chi_{r2,r'2} \equiv \chi_{rr'} \quad (15)$$

$$\mu_{r1} = \mu_{r2} \equiv \mu_r \quad (16)$$

$$\chi_{r1,r2} \equiv \chi_v. \quad (17)$$

Here, χ_v is real and positive, and all other inter-layer χ 's

are assumed to vanish. We let n label the one-particle eigenstates of a single layer, with energies ϵ_n^{2d} . The full one-particle spectrum is then given by

$$\epsilon_{n,\sigma} = \epsilon_n^{2d} + \sigma\chi_v, \quad (18)$$

where $\sigma = \pm 1$. We assume that the energy spectrum and filling are such that only $\sigma = -1$ states are occupied by fermions, in which case the two-dimensional spectrum ϵ_n^{2d} (shifted in energy by $-\chi_v$) is filled by $NN_s/k = 2NN_s^{2d}/k$ fermions. This corresponds to a single-layer problem with twice as many fermions, or filling parameter $k' = k/2$. The saddle point energy is then

$$E_{MFT} = NN_s^{2d} \frac{\chi_v^2}{\mathcal{J}} - \frac{2NN_s^{2d}}{k} \chi_v \quad (19)$$

$$+ \frac{2N}{\mathcal{J}} \sum_{\langle rr' \rangle} |\chi_{rr'}|^2 + m' \sum_r \mu_r + E_f^{2d}(k').$$

Here, $m' = 2m$, and $E_f^{2d}(k')$ is the ground state energy of the fermionic part of the mean-field Hamiltonian [last two terms of Eq. (8)], for a single-layer square lattice with filling parameter k' . The first two terms of Eq. (19) are minimized with respect to χ_v to find $\chi_v = \mathcal{J}/k$. The last three terms combine to $E_{MFT}^{2d}(k', \mathcal{J}')$, the saddle point energy of a single-layer square lattice with filling parameter k' and $\mathcal{J}' = \mathcal{J}/2$. Noting that

$$E_{MFT}^{2d}(k') \equiv E_{MFT}^{2d}(k', \mathcal{J}) = 2E_{MFT}^{2d}(k', \mathcal{J}'), \quad (20)$$

we obtain the following relation between bilayer and single-layer saddle point energies:

$$\frac{E_{MFT}}{N_s N} = -\frac{\mathcal{J}}{2k^2} + \frac{1}{4} \frac{E_{MFT}^{2d}(k/2)}{N_s^{2d} N}. \quad (21)$$

This relation allows us to study via SCM the single-layer square lattice with filling parameter $k' = k/2$ as a further check on the cubic lattice results. For integer k' , this was already done in Ref. 7. We carried out SCM calculations for the half-odd integer filling parameters $k' = \frac{5}{2}, \frac{7}{2}, \frac{9}{2}$ (see Table II and Fig. 3). For all values of k , these calculations find the same ground states as found by the single-bilayer SCM calculations.

As a further check on our results, we also computed the energies of some simple competing states. Table III compares the energies of these states to the ground state saddle point energies found by SCM.

IV. DISCUSSION

The large- N results presented here find a rich variety of candidate non-magnetic ground states for Mott insulators of ultra-cold fermionic AEA. It would be fascinating to realize any of these states experimentally. In order to achieve this, there still need to be substantial advances in preparation of low-entropy magnetic states of ultra-cold atoms, and our results add to the increasing motivation

k	Cubic lattice	Single bilayer	$k/2$ square lattice
5	$1 \leq l_{x,y,z} \leq 5$	10 30	10 60
6	$1 \leq l_{x,y,z} \leq 6$	4 30	4 60
7	$1 \leq l_{x,y,z} \leq 7$	4 21	10 35
8	$1 \leq l_{x,y} \leq 8$ $1 \leq l_z \leq 5$	4 24	4 40
9	$1 \leq l_{x,y} \leq 9$ $1 \leq l_z \leq 4$	4 36	10 36
10	$1 \leq l_{x,y} \leq 10$ $1 \leq l_z \leq 4$	4 30	5 60

TABLE II. This table contains information about our SCM numerical study on the cubic lattice (1st column), as well as the related problems of a single bilayer (2nd column), and single layer square lattice with $k' = k/2$ (3rd column). On the left-hand side of each entry of the table, the range of unit cell dimensions is shown as an inequality. For every choice of $l_{x,y,z}$ within the given range, the number of times we ran the SCM algorithm with distinct random initial configurations of $\chi_{rr'}$ is shown on the right-hand side of the entry (top). Also on the right-hand side is the minimum linear system size L (bottom, italics).

to pursue such advances specifically in AEA systems. In addition, if future experiments can enter a regime where any of the states discussed here can be realized, it will be of crucial importance to devise probes of their characteristic properties.

We would like to close by highlighting the CSL bilayer state, which has some striking properties that would be fascinating to realize experimentally, and which we now briefly discuss. At the large- N mean-field level the cubic lattice breaks into disconnected bilayers, and one can understand the properties beyond mean-field theory by first focusing on a single bilayer. The effect of fluctuations is to couple the fermions to a dynamical $U(1)$ gauge

field. The mean-field fermions are in a gapped integer quantum Hall state, so integrating them out generates a Chern-Simons term for the $U(1)$ gauge field. Because the mean-field fermions in a single bilayer and in the single-layer square lattice CSL^{7,13} have in both cases a single chiral edge mode per spin species, the coefficient of the Chern-Simons term and associated topological properties are the same. The spinons are Abelian anyons with statistics angle $\theta = \pi \pm \pi/N$, and there is a chiral edge mode with gapless excitations carrying $SU(N)$ spin, which is described by a chiral $SU(N)_1$ Wess-Zumino-Witten model.^{7,13}

If adjacent bilayers are coupled weakly, bulk properties are unaffected due to the energy gap. One simply has a many-layer CSL state, with anyonic spinons confined to the individual bilayers. Due to the gapless edge modes of single bilayers, the physics on the two-dimensional surface is likely more interesting. This depends crucially on whether adjacent bilayers have the same or opposite magnetic flux, as the direction of the flux controls the direction of the chiral edge modes. If the fluxes are aligned oppositely in neighboring bilayers, then edge modes on neighboring bilayers are counterpropagating and an energy gap is possible on the two-dimensional surface. On the other hand, if all fluxes are parallel, then all the chiral edge modes propagate in the same direction, and the two-dimensional surface is expected to remain gapless. The resulting surface state is a kind of two-dimensional chiral “spin metal,” which could be interesting to study in future work.

ACKNOWLEDGMENTS

M.H. gratefully acknowledges Victor Gurarie and Ana Maria Rey for related prior collaborations. This work is supported by DOE award no. DE-SC0003910.

¹ D. Jaksch and P. Zoller, *Ann. Phys.* **315**, 52 (2005).

² M. Lewenstein *et al.*, *Advances in Physics* **56**, 243 (2007).

³ I. Bloch, J. Dalibard, and W. Zwerger, *Rev. Mod. Phys.* **80**, 885 (2008).

⁴ We do not consider bosonic AEAs, because all stable bosonic atoms with similar electronic structure have zero nuclear spin.

⁵ A. V. Gorshkov, M. Hermele, V. Gurarie, C. Xu, P. S. Julienne, J. Ye, P. Zoller, E. Demler, M. D. Lukin, and A. M. Rey, *Nat. Phys.* **6**, 289 (2010).

⁶ M. A. Cazalilla, A. F. Ho, and M. Ueda, *New J. Phys.* **11**, 103033 (2009).

⁷ M. Hermele, V. Gurarie, and A. M. Rey, *Phys. Rev. Lett.* **103**, 135301 (2009).

⁸ M. Foss-Feig, M. Hermele, and A. M. Rey, *Phys. Rev. A* **81**, 051603 (2010).

⁹ M. Foss-Feig, M. Hermele, V. Gurarie, and A. M. Rey, *Phys. Rev. A* **82**, 053624 (2010).

¹⁰ C. Xu, *Phys. Rev. B* **81**, 144431 (2010).

¹¹ T. A. Tóth, A. M. Läuchli, F. Mila, and K. Penc, *Phys. Rev. Lett.* **105**, 265301 (2010).

¹² P. Corboz, A. M. Läuchli, K. Penc, M. Troyer, and F. Mila, *Phys. Rev. Lett.* **107**, 215301 (2011).

¹³ M. Hermele and V. Gurarie, *Phys. Rev. B* **84**, 174441 (2011).

¹⁴ S. R. Manmana, K. R. A. Hazzard, G. Chen, A. E. Feiguin, and A. M. Rey, *Phys. Rev. A* **84**, 043601 (2011).

¹⁵ A. Rapp and A. Rosch, *Phys. Rev. A* **83**, 053605 (2011).

¹⁶ G. Szirmai, E. Szirmai, A. Zamora, and M. Lewenstein, *Phys. Rev. A* **84**, 011611 (2011).

¹⁷ B. Bauer, P. Corboz, A. M. Läuchli, L. Messio, K. Penc, M. Troyer, and F. Mila, *Phys. Rev. B* **85**, 125116 (2012).

¹⁸ L. Bonnes, K. R. A. Hazzard, S. R. Manmana, A. M. Rey, and S. Wessel, *Phys. Rev. Lett.* **109**, 205305 (2012).

¹⁹ L. Messio and F. Mila, *Phys. Rev. Lett.* **109**, 205306 (2012).

k	5	6	7	8	9	10
Bilayer ($\Phi = 2\pi n/k$)	-0.0444916	-0.0344012	-0.0273888	-0.0223613	-0.0186271	-0.01577
k -site cluster	-0.04	-0.032407	-0.026239	-0.0234375	-0.0178326	-0.014
Uniform real χ	-0.0394159	-0.0312776	-0.0254048	-0.0210391	-0.0177088	-0.0151133
$(2\pi n_{x,y,z}/k)$ -flux	-0.0430802	-0.0330693	-0.0261299	-0.0212772	-0.0177579	-0.0151134
SCM ground state	-0.0445021	-0.0347222	-0.0273888	-0.0234375	-0.0188265	-0.01577

TABLE III. Comparison of energies of a variety of simple saddle points (top four rows), with the energy of the ground state found by SCM numerics (bottom row). All energies are in units of $N\mathcal{J}N_s$. Each row represents a class of saddle points, described below. For classes including multiple different saddle points, the energy shown is the lowest in the class. We considered the following classes of saddle points: *Bilayer* ($\Phi = 2\pi n/k$). We considered a generalization of the CSL bilayer saddle point described in the main text, where the flux through each plaquette is $\Phi = 2\pi n/k$, where $n = 0, \dots, k-1$. *k-site cluster*. The energy of a cluster with k sites is proportional to the number of bonds in the cluster,^{7,13} so the lowest-energy such state can be found by finding a k -site cluster containing the greatest number of bonds. *Uniform real χ* . This is the state where $\chi_{rr'}$ is real and spatially constant. *$(2\pi n_{x,y,z}/k)$ -flux*. These states have $2\pi n_x/k$ flux through every plaquette normal to the x -direction, and similarly for y and z , where $0 \leq n_{x,y,z} \leq k-1$. Since most of these states break lattice rotation symmetry, the magnitude $|\chi_{rr'}|$ is allowed to vary depending on bond orientation, but is fixed to be translation invariant.⁸⁰

- ²⁰ A. Tokuno and T. Giamarchi, Phys. Rev. A **86**, 053614 (2012).
- ²¹ K. R. A. Hazzard, V. Gurarie, M. Hermele, and A. M. Rey, Phys. Rev. A **85**, 041604 (2012).
- ²² Z. Cai, H.-H. Hung, L. Wang, D. Zheng, and C. Wu, (), arXiv:1202.6323.
- ²³ Z. Cai, H.-H. Hung, L. Wang, Y. Li, and C. Wu, (), arXiv:1207.6843.
- ²⁴ P. Corboz, K. Penc, F. Mila, and A. M. Läuchli, Phys. Rev. B **86**, 041106 (2012).
- ²⁵ P. Corboz, M. Lajkó, A. M. Läuchli, K. Penc, and F. Mila, Phys. Rev. X **2**, 041013 (2012).
- ²⁶ T. Fukuhara, Y. Takasu, M. Kumakura, and Y. Takahashi, Phys. Rev. Lett. **98**, 030401 (2007).
- ²⁷ T. Fukuhara, S. Sugawa, and Y. Takahashi, Phys. Rev. A **76**, 051604 (2007).
- ²⁸ T. Fukuhara, S. Sugawa, M. Sugimoto, S. Taie, and Y. Takahashi, Phys. Rev. A **79**, 041604 (2009).
- ²⁹ Y. N. Martinez de Escobar, P. G. Mickelson, M. Yan, B. J. DeSalvo, S. B. Nagel, and T. C. Killian, Phys. Rev. Lett. **103**, 200402 (2009).
- ³⁰ S. Stellmer, M. K. Tey, B. Huang, R. Grimm, and F. Schreck, Phys. Rev. Lett. **103**, 200401 (2009).
- ³¹ B. J. DeSalvo, M. Yan, P. G. Mickelson, Y. N. Martinez de Escobar, and T. C. Killian, Phys. Rev. Lett. **105**, 030402 (2010).
- ³² S. Taie, Y. Takasu, S. Sugawa, R. Yamazaki, T. Tsujimoto, R. Murakami, and Y. Takahashi, Phys. Rev. Lett. **105**, 190401 (2010).
- ³³ M. K. Tey, S. Stellmer, R. Grimm, and F. Schreck, Phys. Rev. A **82**, 011608 (2010).
- ³⁴ S. Stellmer, M. K. Tey, R. Grimm, and F. Schreck, Phys. Rev. A **82**, 041602 (2010).
- ³⁵ S. Sugawa, K. Inaba, S. Taie, R. Yamazaki, M. Yamashita, and Y. Takahashi, Nat. Phys. **7**, 642 (2011).
- ³⁶ S. Blatt, T. L. Nicholson, B. J. Bloom, J. R. Williams, J. W. Thomsen, P. S. Julianne, and J. Ye, Phys. Rev. Lett. **107**, 073202 (2011).
- ³⁷ M. Bishof, Y. Lin, M. D. Swallows, A. V. Gorshkov, J. Ye, and A. M. Rey, Phys. Rev. Lett. **106**, 250801 (2011).
- ³⁸ M. Bishof, M. J. Martin, M. D. Swallows, C. Benko, Y. Lin, G. Quémener, A. M. Rey, and J. Ye, Phys. Rev. A **84**, 052716 (2011).
- ³⁹ N. D. Lemke, J. von Stecher, J. A. Sherman, A. M. Rey, C. W. Oates, and A. D. Ludlow, Phys. Rev. Lett. **107**, 103902 (2011).
- ⁴⁰ S. Stellmer, R. Grimm, and F. Schreck, Phys. Rev. A **84**, 043611 (2011).
- ⁴¹ S. Stellmer, R. Grimm, and F. Schreck, Phys. Rev. A **87**, 013611 (2013).
- ⁴² I. Affleck and J. B. Marston, Phys. Rev. B **37**, 3774 (1988).
- ⁴³ J. B. Marston and I. Affleck, Phys. Rev. B **39**, 11538 (1989).
- ⁴⁴ N. Read and S. Sachdev, Nucl. Phys. B **316**, 609 (1989).
- ⁴⁵ V. Kalmeyer and R. B. Laughlin, Phys. Rev. Lett. **59**, 2095 (1987).
- ⁴⁶ V. Kalmeyer and R. B. Laughlin, Phys. Rev. B **39**, 11879 (1989).
- ⁴⁷ X. G. Wen, F. Wilczek, and A. Zee, Phys. Rev. B **39**, 11413 (1989).
- ⁴⁸ D. V. Khveshchenko and P. B. Wiegmann, Mod. Phys. Lett. B **3**, 1383 (1989).
- ⁴⁹ D. V. Khveshchenko and P. B. Wiegmann, Mod. Phys. Lett. B **4**, 17 (1990).
- ⁵⁰ H. Yao and S. A. Kivelson, Phys. Rev. Lett. **99**, 247203 (2007).
- ⁵¹ D. F. Schroeter, E. Kapit, R. Thomale, and M. Greiter, Phys. Rev. Lett. **99**, 097202 (2007).
- ⁵² M. Greiter and R. Thomale, Phys. Rev. Lett. **102**, 207203 (2009).
- ⁵³ R. Thomale, E. Kapit, D. F. Schroeter, and M. Greiter, Phys. Rev. B **80**, 104406 (2009).
- ⁵⁴ B. Scharfenberger, R. Thomale, and M. Greiter, Phys. Rev. B **84**, 140404 (2011).
- ⁵⁵ B. Sutherland, Phys. Rev. B **12**, 3795 (1975).
- ⁵⁶ I. Affleck, Nucl. Phys. B **305**, 582 (1988).
- ⁵⁷ C. Honerkamp and W. Hofstetter, Phys. Rev. Lett. **92**, 170403 (2004).
- ⁵⁸ F. F. Assaad, Phys. Rev. B **71**, 075103 (2005).
- ⁵⁹ V. L. Pokrovskii and G. V. Uimin, Sov. Phys. JETP **34**, 457 (1972).
- ⁶⁰ Y. Q. Li, M. Ma, D. N. Shi, and F. C. Zhang, Phys. Rev. Lett. **81**, 3527 (1998).
- ⁶¹ M. van den Bossche, F. C. Zhang, and F. Mila, Eur. Phys. J. B **17**, 367 (2000).
- ⁶² A. Läuchli, F. Mila, and K. Penc, Phys. Rev. Lett. **97**, 087205 (2006).

- ⁶³ D. P. Arovas, Phys. Rev. B **77**, 104404 (2008).
- ⁶⁴ F. Wang and A. Vishwanath, Phys. Rev. B **80**, 064413 (2009).
- ⁶⁵ N. Fukushima, “Vanishing neel ordering of SU(n) heisenberg model in three dimensions,” (2005), arXiv:cond-mat/0502484.
- ⁶⁶ S. Pankov, R. Moessner, and S. L. Sondhi, Phys. Rev. B **76**, 104436 (2007).
- ⁶⁷ C. Xu and C. Wu, Phys. Rev. B **77**, 134449 (2008).
- ⁶⁸ C. Wu, J.-P. Hu, and S.-C. Zhang, Phys. Rev. Lett. **91**, 186402 (2003).
- ⁶⁹ S. Chen, C. Wu, S.-C. Zhang, and Y. Wang, Phys. Rev. B **72**, 214428 (2005).
- ⁷⁰ P. Lecheminant, E. Boulat, and P. Azaria, Phys. Rev. Lett. **95**, 240402 (2005).
- ⁷¹ C. Wu, Phys. Rev. Lett. **95**, 266404 (2005).
- ⁷² C. Wu, Mod. Phys. Lett. B **20**, 1707 (2006).
- ⁷³ C. Wu, Physics **3**, 92 (2010).
- ⁷⁴ E. Szirmai and M. Lewenstein, EPL (Europhysics Letters) **93**, 66005 (2011).
- ⁷⁵ R. Moessner and J. T. Chalker, Phys. Rev. Lett. **80**, 2929 (1998).
- ⁷⁶ For $k = 5, 6$, where we find a continuous ground state degeneracy within each cluster, these statements hold for a particular choice of ground state in each cluster.
- ⁷⁷ D. S. Rokhsar, Phys. Rev. B **42**, 2526 (1990).
- ⁷⁸ W. H. Press, S. A. Teukolsky, W. T. Vetterling, and B. P. Flannery, *Numerical Recipes in C: The Art of Scientific Computing*, 2nd ed. (Cambridge University Press, 1992).
- ⁷⁹ We also considered some more general parallelepiped unit cells, but less systematically than the rectangular prism case.
- ⁸⁰ The calculation procedure is to set up special initial data of $\chi_{rr'}$ for iteration under the SCM procedure. For those $\chi_{rr'} \neq 0$ in a given state, we choose $|\chi_{rr'}| = 0.1$, with the required pattern of fluxes. After finding the lowest energy, we checked whether the flux pattern is preserved. For $(2\pi n_{x,y,z}/k)$ -flux states, when $k \geq 7$ the computation time becomes large, so we restricted the range of flux to $0 \leq n_x \leq 1$, and $0 \leq n_{y,z} \leq k - 1$.